# Imaging of Triglycerides in Tissues Using Nanospray Desorption Electrospray Ionization (Nano-DESI) Mass Spectrometry

Daisy Unsihuay¹, Jiamin Qiu², Sneha Swaroop¹‡, Konstantin O. Nagornov,³ Anton N. Kozhinov,³ Yury O. Tsybin,³ Shihuan Kuang ² and Julia Laskin¹□

- 1. Department of Chemistry, Purdue University, West Lafayette, IN 47907, USA
- 2. Department of Animal Sciences, Purdue University, West Lafayette, IN 47907, USA
- 3. Spectroswiss, EPFL Innovation Park, 1015 Lausanne, Switzerland

Corresponding author: Julia Laskin, Tel: 765-494-5464, Email: <a href="mailto:jlaskin@purdue.edu">jlaskin@purdue.edu</a>

-

<sup>&</sup>lt;sup>‡</sup> An undergraduate student researcher.

#### **Abstract**

Nonpolar triglycerides (TGs) are rarely detected in mass spectrometry imaging (MSI) experiments unless they are abundant in the sample. Herein, we use nanospray desorption electrospray ionization (nano-DESI) to explore the role of the solvent composition and ionic dopants on the detection of TGs in a murine gastrocnemius muscle tissue used as a model system. We evaluated three solvent mixtures for their ability to extract nonpolar TG species: MeOH:H<sub>2</sub>O 9:1 (v/v), MeOH:DCM 6:4 (v/v) and MeOH:AcN:tol 5:3.5:1.5 (v/v/v). We observe that TGs are mainly detected as [M+K]<sup>+</sup> adducts and their extraction efficiency is improved using less polar solvents: MeOH:DCM and MeOH:AcN:tol . We also explore whether the ionization efficiency of TGs may be improved by doping the MeOH:AcN:tol solvent with ammonium formate (AF) and other ionic additives. However, the formation of [M+NH<sub>4</sub>]<sup>+</sup> adducts of TGs is less efficient than the formation of [M+K]<sup>+</sup> adducts in the range of AF concentrations from 0.1 to 10 mM. Chemical derivatization using 100 µM of Girard T reagent predominately generates reaction products of phosphatidylcholine rather than TG species. Moreover, the presence of the Girard T reagent suppresses ion signals of all the species in the spectrum including TGs. Nano-DESI MSI experiments performed using MeOH:AcN:tol solvent enable imaging of TGs without any detectable adverse effect on signals of other lipids and metabolites. Specifically, 10 out of 14 TG species were detected exclusively using MeOH:AcN:tol and the sensitivity towards other TGs was improved by at least an order of magnitude. Although polyunsaturated TGs may be detected using both solvents, saturated and monounsaturated TGs are only detected using MeOH:AcN:tol. Our results provide a direct path for the improved detection of TGs in tissue imaging experiments using liquid-based ambient ionization techniques.

#### 1. Introduction

Lipids play an important role in biological systems by participating in signaling and energy storage and serving as cell membrane components [1]. Their complexity and structural diversity have always presented a challenge for both qualitative and quantitative analysis. At present, liquid chromatography coupled to mass spectrometry (LC-MS) is by far the most common platform used in lipidomics studies [2,3]. LC-MS approaches have enabled confident identification and detection of both high- and low-abundance analytes in complex lipid mixtures. Alternatively, shotgun lipidomics approaches have been developed in an effort to improve the analysis throughput [4–6].

Mass spectrometry imaging (MSI) also has emerged as a powerful tool for the spatial mapping of molecules in biological samples [7–9]. MSI is a label-free technology, which simultaneously provides chemical and spatial information in the form of molecular images. When used for lipid imaging, MSI experiments may be described as spatially-resolved shotgun lipidomics. Matrix assisted laser desorption/ionization (MALDI) is the most common ionization technique used for the imaging of a broad range of analytes ranging from small lipids and metabolites [10] to large biomolecules such as intact proteins [11]. Ambient liquid extraction ionization techniques including desorption electrospray ionization (DESI) and nanospray desorption electrospray ionization (nano-DESI) are gaining popularity in MSI because they operate under open-air conditions and do not require sample preparation [12–15]. The application of these techniques to tissue imaging provides insights into the specific functions of lipids and metabolites in biological systems and helps identify potential biomarkers for the study of disease mechanisms [16-19]. One of the advantages of ambient liquid extraction techniques is that solvent composition can be tailored to either enable selective extraction of the analytes of interest or provide broad coverage of molecules in the sample [13]. Moreover, the addition of dopants to the working solvent has proven to be successful to improve the extraction of low-solubility species [20] or enhance the ionization by changing the polarity of the analyte [21,22]. In DESI experiments, binary mixtures of water with methanol (MeOH) at different ratios were reported to be suitable for the analysis of different phospholipid classes and sphingolipids [23]. A mixture of dimethylformamide (DMF) with water or acetonitrile (AcN) has been used in DESI MSI experiments as a less destructive and tissue friendly solvent, which helped improved the sensitivity of the technique towards small metabolites [24].

In nano-DESI, molecules from the sample are extracted into a liquid bridge formed between two glass capillaries [25,26], transferred to a mass spectrometer inlet, and ionized by electrospray ionization. A majority of nano-DESI MSI experiments reported so far have been performed using a solvent composed of MeOH:H<sub>2</sub>O (9:1) (v/v), which provides good coverage for most of lipid classes [18,27]. It is not surprising that due to the polar nature of these traditionally used solvents, polar lipids were predominately observed in these studies. However, triglycerides (TGs) are detected with low efficiency using this solvent composition. Indeed, direct comparison between nano-DESI MSI and LC-MS/MS lipidomics analysis performed using MeOH:H<sub>2</sub>O (9:1) revealed good coverage of a majority of lipid classes except for TGs in nano-DESI MSI [28].

TGs are neutral lipids consisting of a glycerol backbone and three fatty acyl chains. In mammals, TGs serve as the main source of energy for the body. Indeed, oxidation of TGs releases more than twice as much energy per gram than other biomolecules such as carbohydrates and proteins [29]. Accumulation of TGs in non-adipose tissues is associated with the development of insulin resistance [30] as well as other pathologies [31,32]. Therefore, the ability to explore the localization of TGs in tissue sections is important for understanding of their role in complex biological processes. Nonpolar TGs are not readily extracted and ionized, which presents a challenge for imaging experiments utilizing liquid extraction-based ionization techniques. Therefore, it is important to develop approaches to improve their detection in these experiments. DESI analysis of TGs using 1:1 water/methanol (v/v) was performed for samples rich in TGs including edible oils and margarines [33]. However, DESI imaging of TGs was reported for the first time after their complexation with Ag+ ions which improved the detection of olefinic lipids [34]. This method allowed the detection of unsaturated but not of saturated TGs, which do not contain double bonds known to interact with Ag+ ions.

In this work, we aim to address the limitation of the 9:1 (v/v) MeOH:H<sub>2</sub>O system [28], which shows low sensitivity towards neutral TG species. In particular, we explore the effect of solvent composition on the extraction and ionization of TGs using gastrocnemius muscle tissue as a model system. We hypothesized that extraction of TGs may be improved using non-polar organic solvents and compared the detection efficiency of TGs using three solvent mixtures containing nonpolar components. Furthermore, we examined the effect of ionic and reactive dopants on the ionization efficiency of TGs. Our results demonstrate substantial improvement in the detection of TGs as [M+K]<sup>+</sup> species using less polar solvents. However, we did not observe an improvement in the ionization efficiency using ionic dopants in the solvent. This is attributed to the high content of K<sup>+</sup> ions in tissue samples and favorable cationization of TGs via potassium cation complexation making [M+K]<sup>+</sup> adducts of TGs the most abundant species in the spectrum. On-line chemical derivatization with Girard T (GT) performed on the tissue did not produce reaction products with

TGs on the timescale of nano-DESI analysis. Nano-DESI MSI experiments carried out using methanol:acetonitrile:toluene mixture enabled imaging of at least fourteen TG species in the tissue without noticeably affecting the detection efficiency of other analytes in the tissue. This result suggests that the detection of TGs in tissue sections using liquid extraction techniques is mainly determined by their solubility in the extraction solvent.

## 2. Materials and methods

#### 2.1. Chemicals and solutions

Ammonium formate (AF) and HPLC plus toluene (tol) were acquired from Sigma-Aldrich. Omnisolv LC-MS grade water, methanol (MeOH), and acetonitrile (AcN) were purchased from Millipore Sigma's (Burlington, MA). Dichloromethane (DCM) (≥ 99.5% purity) was purchased from Avantor (Radnor, PA). Solvent mixtures used in this study are comprised of: (1) a 9:1 (v/v) MeOH:H<sub>2</sub>O mixture, (2) a 5:3.5:1.5 (v/v/v) MeOH:AcN:tol and (3) a 6:4 (v/v) MeOH:DCM mixture. A 100 µM solution of Girard T and AF solutions with concentrations ranging from 0.1 to 10 mM were also prepared using MeOH:AcN:tol.

## 2.2. Tissue collection and handling

Adult (3-month old) C57BL/6 mice used in this study were originally obtained from Jackson Laboratory (Bar Harbor, ME) and maintained in the animal facility with free access to standard rodent chow and water. All the procedures involving mice were approved by the Purdue University Animal Care and Use Committee (Protocol# 1112000440). Gastrocnemius muscles were collected as previously described [35]. Samples were flash frozen in liquid nitrogen, embedded using the optimal cutting temperature compound (OCT compound) with 1/2 of tissue devoid of OCT, and stored in a -80°C freezer. Regions of the frozen muscle tissues remote from the OCT embedding were cross sectioned serially into 10 µm-thick sections using a Leica CM1850 cryostat. Adjacent sections were attached onto glass slides and stored in a slide storage box at -80°C. Tissue sections were allowed to thaw at room temperature prior running nano-DESI MSI experiments.

### 2.3. Nano-DESI analysis

Individual line scans using different solvent compositions were acquired using an Agilent 6560 IM-QTOF MS (Agilent Technologies, Santa Clara), whereas imaging experiments were performed on a Q-Exactive HF-X Orbitrap mass spectrometer (Thermo Fisher Scientific, Waltham, MA) using a custom designed nano-DESI source [27,36]. The nano-DESI probe was assembled by forming a liquid bridge between the primary and nanospray fused silica capillaries (OD 150µm x ID 50µm).

The nanospray capillary delivered the extracted analytes to the mass spectrometer inlet where they were ionized using electrospray ionization. A detailed description of this custom-designed shear force measurement unit can be found in our previous papers [36,37]. A third fused silica capillary (200 μm ID, 790 μm OD) was pulled to ~20 μm OD using a P-2000 puller (Sutter instrument, Novato, CA) to serve as a shear force probe. Pulling parameters: Line 1, Heat 650, Fil 4, Vel 80, Del 130, Pull 60; Line 2, Heat 650, Fil 4, Vel 50, Del 130, Pull 60. Two piezoelectric ceramic plates (3.8 MHz, Steiner & Martins, Inc., Doral, FL) were attached to the shear force probe: the upper plate induced the probe oscillation using a function generator and the bottom plate positioned closer to the sample, detected the amplitude of the shear force vibration through a lock-in amplifier (Stanford Research Systems, Sunnyvale, CA). The shear force probe was positioned next to the nano-DESI probe to maintain a constant distance between the sample and the nano-DESI probe and therefore, the same extraction efficiency throughout the experiment. All capillaries were positioned in front of the mass spectrometer inlet using high-resolution micromanipulators (5, XYZ500TIM, Quater Research and Development, Bend, OR). Two Dino-Lite microscope cameras were used to guide the assembly of the nano-DESI and shear force probes.

Two solvent compositions were used in imaging experiments: (1) MeOH:H<sub>2</sub>O (9:1) (v/v) and (2) MeOH:AcN:tol (5:3.5:1.5) (v/v/v). These solvents were infused using a syringe pump at 0.5  $\mu$ L/min. Ionization was achieved by applying a 3.5 kV potential to the syringe needle. The heated capillary inlet was held at 30 V and 250 °C. Imaging data were acquired at a scan rate of 40  $\mu$ m/s and a step between the lines of 175  $\mu$ m. Mass spectra were acquired in positive mode in the range of m/z 133–2000. The spatial resolution was kept at ~200  $\mu$ m. Data-dependent MS/MS experiments of molecules extracted from the tissue sections were performed using a mass resolution (m/ $\Delta$ m) of 60,000 at m/z 200, mass isolation window of 0.5 m/z, and HCD energy of 25 arbitrary units specific to the instrument.

### 2.4. Data analysis

Each line scan was collected as an individual file (reduced profile, .RAW file format). Data processing was performed using Peak-by-Peak software (Spectroswiss, Lausanne, Switzerland). Ion images were generated using parallel (multi-core) calculations. First, peaks were extracted from mass spectra using a three-point quadratic interpolation to determine the apex of the peak. Second, peak abundances in each pixel of the image were normalized to the total ion current (TIC = sum of intensities):  $Int_{norm} = (Int_i / \Sigma Int_i)^* 100\%$ . We note that normalization to the abundance of a specified m/z in the spectrum also is enabled by the software. Finally, ion images were

constructed by plotting normalized abundances of targeted m/z features in each mass spectrum (pixel) within the mass tolerance window of ±10 ppm as a function of location on the tissue sample. Initial lipid identification was performed using LIPID MAPS (<a href="www.lipidmaps.org">www.lipidmaps.org</a>) and metabolite identification was performed using METLIN database (<a href="https://metlin.scripps.edu">https://metlin.scripps.edu</a>). Final assignments were performed based on the MS/MS analysis.

Region of interest (ROI) analyses were performed on the regions where TGs were abundant in the tissue. Averaged mass spectra were obtained by spectral averaging over the ROIs and normalized to the TIC obtained over the ROI. The effect of the solvent composition was assessed by comparing the average intensities of TGs normalized to the TIC.

## 3. Results and discussion

In this study, we examined the effect of the solvent composition on the extraction and ionization of TGs in nano-DESI experiments. First, the molecular coverage of the commonly used nano-DESI solvent, MeOH:H<sub>2</sub>O 9:1 (v/v), was compared against two alternative solvents MeOH:AcN:tol 5:3.5:1.5 (v/v/v) and MeOH:DCM 6:4 (v/v). Second, adduct formation and chemical derivatization with Girard T approaches were explored for improving the ionization of TGs. Finally, nano-DESI imaging experiments were performed using MeOH:H<sub>2</sub>O and MeOH:AcN:tol to test the imaging capabilities of these solvents.

## 3.1. Effect of solvent composition on the extraction of TGs

Two alternative solvents were examined for the analysis of TGs using nano-DESI MSI: MeOH:DCM 4:6 (v/v) and MeOH:AcN:tol 5:3.5:1.5 (v/v/v). The first solvent has been previously used in lipidomics analysis of plant and animal tissue samples and provided good coverage of both polar and nonpolar lipids including TGs [38]. The second solvent has been used for the detection of hydrophobic compounds in biological samples [26,39]. However, no systematic study has been reported on the solvent optimization for tissue imaging experiments. **Figure 1a-c** shows average mass spectra obtained for each solvent by acquiring line scans over the central region of the gastrocnemius muscle tissue as illustrated in **Figure 1a**. The results indicate that regardless of the solvent composition, PC species detected in muscle tissue in the mass range of m/z 740-860 as [M+H]+, [M+Na]+ and [M+K]+ adducts are the dominant peaks in positive mode nano-DESI. This observation may be attributed to the polarity of PC species, which facilitates their detection in a mass spectrometer as compared to TGs that are neutral molecules. Moreover, PCs are

mainly membrane lipids and therefore are present in high abundance in tissue samples making them relatively easy to detect.

Although the overall appearance of mass spectra obtained using three different solvents is similar, we observed interesting differences at m/z > 840 (Figure 1c). Specifically, the signals of TGs observed using MeOH:DCM and MeOH:AcN:tol showed an increase in abundance by at least an order of magnitude in comparison with the signals obtained using MeOH:H2O. In the spectra, TGs were mainly detected as [M+K]\* ions while the corresponding [M+Na]\* adducts were much less abundant. This result reflects the important role that the solvent composition plays in ambient ionization techniques based on liquid extraction, in which the solubility of the analyte in the extraction solvent determines how effectively it is partitioned into the solvent. We have previously demonstrated that a 70:30 mixture of acetonitrile and toluene facilitates the extraction and ionization of nonpolar analytes from crude oil samples in nano-DESI experiments [40]. It is reasonable to assume that the nonpolar components such as toluene and DCM improve the extraction efficiency of nonpolar molecules such TGs of interest to this study. Meanwhile, the presence of polar solvents such as MeOH and AcN promotes the extraction of polar lipids and provides a stable electrospray signal [41]. In summary, we observed a comparable performance of the toluene and DCM mixtures in the analysis of muscle tissue sections. In contrast, analysis of mouse liver tissue sections indicated clear differences between these two solvent mixtures. Figure S1a shows regions of the tissue that where sampled using different solvent mixtures by acquiring one line scan for each solvent in each region; Figure S1b shows representative average mass spectra obtained in the adjacent line scans. The MeOH:AcN:tol clearly outperformed MeOH:DCM in all the acquired line scans. Based on these results and safety concerns associated with DCM due to its carcinogenic properties, we chose MeOH:AcN:tol as the working solvent for the following experiments.

## 3.2. Effect of ionization on the detection of TGs

In addition to improving the extraction efficiency of TGs in nano-DESI experiments by optimizing the solvent composition, we explored the effect of different dopants in the solvent on the ionization efficiency of these lipids. Cationization of TG species with ammonium acetate (AA) is a common strategy used in many lipidomics studies to enhance the ionization efficiency of neutral lipids [42,43]. In this study, nano-DESI spectra were acquired using MeOH:AcN:tol solvent containing ammonium formate (AF) at different concentrations in a range of 0.1-10 mM. Representative mass spectra obtained using 0, 0.1 and 2 mM concentration of AF are shown in Figure 2. We observe that the signals corresponding to [M+Na]<sup>+</sup> and [M+K]<sup>+</sup> adducts of PC

species are largely unaffected by the presence of AF in the solvent. The abundance of protonated PC species increases in the presence of AF (**Figure 2b**). This is the only substantial difference between mass spectra obtained at 0 and 0.1 mM AF concentrations (**Figures 2a-b**). Ammonium adducts of TGs appear as low-abundance species at low AF concentration (**Figure 2b**) and increase in abundance at higher AF concentration (**Figure 2c**). However, the abundance of [M+NH<sub>4</sub>]<sup>+</sup> ions of TGs at 2 mM AF concentration is still lower than the abundance of the corresponding [M+K]<sup>+</sup> species. Interestingly, the abundance of [M+K]<sup>+</sup> adducts of TGs increases with an increase in AF concentration. The relatively inefficient ionization of TGs as [M+NH<sub>4</sub>]<sup>+</sup> ions observed in this study may be attributed to the high concentration of potassium ions in the tissue that leads to the preferred formation of [M+K]<sup>+</sup> adducts. Compared with LC-MS analysis where high concentrations of AA are commonly used for lipid profiling, we found that at high concentrations of AF (~10 mM) all the signals were substantially suppressed. Similarly, we did not observe any measurable improvement in the signal of TGs by adding either LiNO<sub>3</sub> or KNO<sub>3</sub> to the solvent. Collectively, these results indicate that the addition of salts to the nano-DESI solvent does not improve the ionization of TGs extracted from muscle tissues.

We also examined whether reactive nano-DESI could be used for the analysis of TGs. On-line chemical derivatization is one of the common strategies used to improve the ionization of neutral molecules [44]. For example, reactive DESI employing betaine aldehyde (BA) as a reagent has been successfully used to improve the detection of cholesterol in brain [44]. This method exploited the reaction between the alcohol group of cholesterol with BA to produce a positively charged hemiacetal. Meanwhile, Girard T (GT) reagent has been used for reactive DESI analysis of ketosteroids [45] and nano-DESI analysis of aldehydes and ketones in organic aerosols [46]. Unlike cholesterol, TGs do not have any functional groups specific to their structure that can be targeted by reactive analysis. However, similar to phospholipids, the carbonyl group of the glycerol backbone can serve as a possible target. Herein, we used GT dissolved in the MeOH:AcN:tol mixture to explore whether reactive nano-DESI analysis will enhance the detection efficiency of TGs in complex mixtures. GT converts aldehydes and ketones into hydrazines by reacting with carbonyl groups [45]. In our experiments, we varied the concentration of GT in the solvent and examined the distribution of m/z features observed in nano-DESI spectra of tissue samples. Although we did not observe any products of reaction between GT and TGs, formation of GT adducts of PC species with ~10% reaction efficiency was observed at GT concentrations above 100 µM. As shown in Figure S2, at this concentration the ion at m/z 132.11 corresponding to the unreacted GT dominates the spectrum obscuring the detection of lower abundance species. Furthermore, the incomplete conversion of PCs into their corresponding hydrazine products

generates a more complicated spectrum, which is not desirable for imaging experiments. In conclusion, neither cationization nor on-line chemical derivatization improved the sensitivity of TG detection in nano-DESI analysis of tissue sections. We conclude that high affinity of TGs towards K<sup>+</sup> ions present in the tissue promotes their ionization and detection in nano-DESI MSI experiments. As a result, no ionization enhancers were used in the imaging experiments described in the next section.

# 3.3. Nano-DESI MSI of gastrocnemius tissues

Two solvents, MeOH:H<sub>2</sub>O and MeOH:AcN:tol, were used to image two adjacent gastrocnemius tissue sections to compare TG detection in nano-DESI MSI experiments. Figure 3a shows optical images of the sections along with ion images of [M+K]+ ions of endogenous phospholipids including LPC(16:0), PC(36:1) and PC(40:6). Ion images corresponding to small metabolites including carnosine and miristoylcarnitine, CAR(14:0), are displayed as [M+K]<sup>+</sup> and [M+H]<sup>+</sup> ions respectively. All ion images are normalized to the total ion current (TIC). In both solvents, the distribution of a majority of phospholipids and metabolites detected in nano-DESI MSI experiments exhibit the same localization and similar abundance. Signaling molecules including LPC(16:0) are evenly distributed across the tissue whereas CAR(14:0), PC(36:1) and PC(40:6) are observed in higher abundance in the deep region of gastrocnemius muscle tissue. Although correlating the localization of these molecules to different types of fibers is out of the scope of this work, it can be suggested that this region is enhanced in oxidative fibers (type I and IIa) based on similar results reported in previous studies using MALDI imaging [47,48]. In contrast, the ion image corresponding to carnosine displayed higher abundance in regions where CAR(14:0), PC(36:1) and PC(40:6) are depleted, suggesting that carnosine may be used as a molecular marker of a different fiber type.

**Figure 3b** shows ion images of representative [M+K]<sup>+</sup> ions of TG species normalized to the TIC. Ion images of other TGs identified in this experiment are shown in **Figure S3**. We note that MS/MS spectra of the [M+K]<sup>+</sup> adducts of TGs did not provide any structural information (**Figure S4**) most likely because of the loss of K<sup>+</sup> ion, which cannot be detected in these experiments. Acyl chain information could only be obtained from the corresponding [M+Na]<sup>+</sup> adducts. Fragmentation of [M+Na]<sup>+</sup> ions suggested the presence of multiple isomers. For example, the MS/MS spectrum of TG(52:4) at m/z 877.725 contained fragment ions corresponding to the loss of the fatty acyl chains FA(18:1), FA(18:2), FA(18:3) and FA(16:0), indicating that the ion image of TG(52:4) is a combination of TG(18:2/18:2/16:0), TG(18:2/18:1/16:1), and TG(18:3/18:1/16:0) isomers (**Figure S5**). Since the signals of the [M+Na]<sup>+</sup> adducts were not as abundant as the [M+K]<sup>+</sup> adducts, we

could not obtain MS/MS of the less abundant TG(46:0), TG(46:1) and TG(48:0) species. Overall, we estimate that we were able to detect 22 different TG species (including possible isomers) using MeOH:AcN:tol. A complete list of all TG species detected is provided in **Table S1**. In the future, we will use MS/MS imaging to examine the spatial localization of isomeric TG species [49].

It can be observed in **Figure 3b** that ion signals of all the TGs are notably higher when MeOH:AcN:tol is used as a working solvent. Polyunsaturated species such as TG(50:2) and TG(52:3) are detected using both solvents. In contrast, the detection of monounsaturated and saturated species such as TG(46:0), TG(48:0) and TG(50:1) and species with longer acyl chains such as TG(54:4) is substantially improved using MeOH:AcN:tol. These results demonstrate better performance of MeOH:AcN:tol solvent for imaging of hydrophobic molecules in tissues.

Region of interest (ROI) analysis was carried out to assess the extraction efficiency of TGs from tissue samples using MeOH:AcN:tol and MeOH:H2O. Figure 4a displays ion images of TG(52:4) obtained using both solvents showing the regions selected for the ROI analysis. The relative abundance of all TG species obtained from the average spectra of the ROI is reported for both solvents in Figure 4b (left axis) along with the ratio of signal intensities, Int<sub>MeOH:H2O</sub>/ Int<sub>MeOH:AcN:tol</sub>, which is plotted against the right axis. We observed higher signals of the more polar unsaturated species in comparison to less polar saturated species. Moreover, higher signals were generally observed for unsaturated TG species with 50 and 52 carbons than for unsaturated TG with 54 carbons (Figure 4b). This observation is consistent with a previous study that discussed the effect of the polarity of acylglycerols on the signals of TGs electrosprayed using nonpolar solvents [50]. Specifically, that study reported higher MS signals of the more polar acylglycerols. Interestingly, less polar TGs are more strongly suppressed in the polar MeOH:H<sub>2</sub>O solvent. For example, we observed similar abundances for TG(50:1) and TG(52:4) in MeOH:AcN:tol. However, TG(50:1) completely disappears when MeOH:H<sub>2</sub>O is used as a working solvent. The intensity ratio, Int<sub>MeOH:H2O</sub>/ Int<sub>MeOH:AcN:tol</sub>, shown in **Figure 4b** indicates that this trend is consistent across all the TG species observed in this study. This result demonstrates the strong influence of the number of double bonds on the extraction efficiency of TG species from tissues in nano-DESI MSI experiments. In particular, the more polar compounds such as TG(52:3) can be extracted using both solvents and more hydrophobic compounds such as TG(46:1) are better extracted using the more hydrophobic solvent. In summary, we obtained good-quality images for 14 distinct m/z of TG species corresponding to at least 22 unique TGs using MeOH:AcN:tol solvent as compared to only four TG images obtained using MeOH:H<sub>2</sub>O. Moreover, the signal intensity of all the TGs was enhanced by at least a factor of 16 in MeOH:AcN:tol.

#### 4. Conclusions

In this study, we examine the effect of extraction and ionization on the detection of TGs in tissue imaging experiments using nano-DESI. We conclude that detection of TGs in these experiments is mainly determined by the extraction efficiency from the sample. Subsequent ionization of TG species is promoted by alkali metal cations that are abundant in biological tissues. The presence of a small fraction of a nonpolar solvent in the solvent mixture has no measurable effect on the signal stability and total ion signal. However, an improved lipid coverage is observed using solvents containing non-polar components, which enable the simultaneous detection of polar and nonpolar lipids in the same experiment. We note that the addition of salts or the GT reagent does not improve the detection of TG species. Imaging experiments confirm that the 5:3.5:1.5 MeOH:AcN:tol mixture provides substantially better coverage of TGs in muscle tissue samples in comparison with the more polar 9:1 MeOH:H<sub>2</sub>O mixture. Ion signals of TGs are improved by at least a factor of 16 allowing imaging of 14 TG species using this solvent in comparison with only four TG species imaged generated using MeOH:H<sub>2</sub>O Meanwhile, similar spatial distributions of metabolites including acylcarnitines, carnosine and PC species were observed using MeOH:H<sub>2</sub>O and MeOH:AcN:tol. Collectively, these results indicate the superior performance of MeOH:AcN:tol in nano-DESI MSI experiments.

## 5. Acknowledgements

This research is supported by the grant from the National Science Foundation (NSF-1808136, JL) and National Institute of Health (R01AR071649, SK). We thank Bingming Chen from Merck for generously providing mouse liver tissue sections.

#### 6. Competing Interests:

The authors declare no competing interests

#### 7. References

- [1] E. Muro, G.E. Atilla-Gokcumen, U.S. Eggert, Lipids in cell biology: how can we understand them better?, Molecular Biology of the Cell. (2014). doi:10.1091/mbc.e13-09-0516.
- [2] T. Cajka, O. Fiehn, Toward Merging Untargeted and Targeted Methods in Mass Spectrometry-Based Metabolomics and Lipidomics, Analytical Chemistry. (2016). doi:10.1021/acs.analchem.5b04491.

- [3] Y.H. Rustam, G.E. Reid, Analytical Challenges and Recent Advances in Mass Spectrometry Based Lipidomics, Analytical Chemistry. (2018). doi:10.1021/acs.analchem.7b04836.
- [4] X. Han, R.W. Gross, Shotgun lipidomics: Electrospray ionization mass spectrometric analysis and quantitation of cellular lipidomes directly from crude extracts of biological samples, Mass Spectrometry Reviews. (2005). doi:10.1002/mas.20023.
- [5] O. Vvedenskaya, Y. Wang, J.M. Ackerman, O. Knittelfelder, A. Shevchenko, Analytical challenges in human plasma lipidomics: A winding path towards the truth, TrAC Trends in Analytical Chemistry. (2018). doi:10.1016/j.trac.2018.10.013.
- [6] X. Han, Lipidomics for studying metabolism, Nature Reviews Endocrinology. (2016). doi:10.1038/nrendo.2016.98.
- [7] J.L. Norris, R.M. Caprioli, Imaging mass spectrometry: A new tool for pathology in a molecular age, Proteomics Clinical Applications. (2013). doi:10.1002/prca.201300055.
- [8] D. Gode, D.A. Volmer, Lipid imaging by mass spectrometry-a review, Analyst. (2013). doi:10.1039/c2an36337b.
- [9] L.A. McDonnell, R.M.A. Heeren, Imaging mass spectrometry, Mass Spectrometry Reviews. (2007). doi:10.1002/mas.20124.
- [10] K.A. Zemski Berry, J.A. Hankin, R.M. Barkley, J.M. Spraggins, R.M. Caprioli, R.C. Murphy, MALDI imaging of lipid biochemistry in tissues by mass spectrometry, Chemical Reviews. (2011). doi:10.1021/cr200280p.
- [11] D.S. Cornett, M.L. Reyzer, P. Chaurand, R.M. Caprioli, MALDI imaging mass spectrometry: Molecular snapshots of biochemical systems, Nature Methods. (2007). doi:10.1038/nmeth1094.
- [12] C. Wu, A.L. Dill, L.S. Eberlin, R.G. Cooks, D.R. Ifa, Mass spectrometry imaging under ambient conditions, Mass Spectrometry Reviews. 32 (2013) 218–243. doi:10.1002/mas.21360.
- [13] J. Laskin, I. Lanekoff, Ambient Mass Spectrometry Imaging Using Direct Liquid Extraction Techniques, Analytical Chemistry. (2016). doi:10.1021/acs.analchem.5b04188.
- [14] R. Javanshad, A.R. Venter, Ambient ionization mass spectrometry: Real-time, proximal sample processing and ionization, Analytical Methods. (2017). doi:10.1039/c7ay00948h.
- [15] C.J. Perez, A.K. Bagga, S.S. Prova, M. Yousefi Taemeh, D.R. Ifa, Review and perspectives on the applications of mass spectrometry imaging under ambient conditions, Rapid Communications in Mass Spectrometry. (2018). doi:10.1002/rcm.8145.
- [16] L.S. Eberlin, I. Norton, A.L. Dill, A.J. Golby, K.L. Ligon, S. Santagata, R. Graham Cooks, N.Y.R. Agar, Classifying human brain tumors by lipid imaging with mass spectrometry, Cancer Research. (2012). doi:10.1158/0008-5472.CAN-11-2465.
- [17] J. Zhang, W. Yu, S.W. Ryu, J. Lin, G. Buentello, R. Tibshirani, J. Suliburk, L.S. Eberlin, Cardiolipins are biomarkers of mitochondria-rich thyroid oncocytic tumors, Cancer Research. (2016). doi:10.1158/0008-5472.CAN-16-1545.
- [18] I. Lanekoff, J. Cha, J.E. Kyle, S.K. Dey, J. Laskin, K.E. Burnum-Johnson, Trp53 deficient mice predisposed to preterm birth display region-specific lipid alterations at the embryo

- implantation site, Scientific Reports. (2016). doi:10.1038/srep33023.
- [19] H.M. Bergman, L. Lindfors, F. Palm, J. Kihlberg, I. Lanekoff, Metabolite aberrations in early diabetes detected in rat kidney using mass spectrometry imaging, Analytical and Bioanalytical Chemistry. (2019). doi:10.1007/s00216-019-01721-5.
- [20] R. Javanshad, E. Honarvar, A.R. Venter, Addition of Serine Enhances Protein Analysis by DESI-MS, Journal of the American Society for Mass Spectrometry. (2019). doi:10.1007/s13361-018-02129-8.
- [21] D. Lostun, C.J. Perez, P. Licence, D.A. Barrett, D.R. Ifa, Reactive DESI-MS Imaging of Biological Tissues with Dicationic Ion-Pairing Compounds, Analytical Chemistry. (2015). doi:10.1021/ac5042445.
- [22] K.D. Duncan, R. Fang, J. Yuan, R.K. Chu, S.K. Dey, K.E. Burnum-Johnson, I. Lanekoff, Quantitative Mass Spectrometry Imaging of Prostaglandins as Silver Ion Adducts with Nanospray Desorption Electrospray Ionization, Analytical Chemistry. (2018). doi:10.1021/acs.analchem.8b00350.
- [23] N.E. Manicke, J.M. Wiseman, D.R. Ifa, R.G. Cooks, Desorption Electrospray Ionization (DESI) Mass Spectrometry and Tandem Mass Spectrometry (MS/MS) of Phospholipids and Sphingolipids: Ionization, Adduct Formation, and Fragmentation, Journal of the American Society for Mass Spectrometry. (2008). doi:10.1016/j.jasms.2007.12.003.
- [24] L.S. Eberlin, C.R. Ferreira, A.L. Dill, D.R. Ifa, L. Cheng, R.G. Cooks, Nondestructive, Histologically Compatible Tissue Imaging by Desorption Electrospray Ionization Mass Spectrometry, ChemBioChem. (2011). doi:10.1002/cbic.201100411.
- [25] P.J. Roach, J. Laskin, A. Laskin, Nanospray desorption electrospray ionization: An ambient method for liquid-extraction surface sampling in mass spectrometry, Analyst. (2010). doi:10.1039/c0an00312c.
- [26] J. Laskin, B.S. Heath, P.J. Roach, L. Cazares, O.J. Semmes, Tissue imaging using nanospray desorption electrospray ionization mass spectrometry, Analytical Chemistry. (2012). doi:10.1021/ac2021322.
- [27] I. Lanekoff, B.S. Heath, A. Liyu, M. Thomas, J.P. Carson, J. Laskin, Automated platform for high-resolution tissue imaging using nanospray desorption electrospray ionization mass spectrometry, Analytical Chemistry. (2012). doi:10.1021/ac301909a.
- [28] S.N. Nguyen, J.E. Kyle, S.E. Dautel, R. Sontang, T. Luders, R. Corley, C. Ansong, J. Carson, J. Laskin, Lipids Extraction study of Lung Tissue by Nano-DESI MS Imaging and LC-MS/MS Lipidomic, Analytical Chemistry. (2019) submitted.
- [29] L.S. J. Berg, J. Tymoczko, Biochemistry, 5th ed., W.H. Freeman, New York, 2002.
- [30] A. Lettner, M. Roden, Ectopic fat and insulin resistance, Current Diabetes Reports. (2008). doi:10.1007/s11892-008-0032-z.
- [31] M. Schweiger, A. Lass, R. Zimmermann, T.O. Eichmann, R. Zechner, Neutral lipid storage disease: genetic disorders caused by mutations in adipose triglyceride lipase/PNPLA2 or CGI-58 / ABHD5, American Journal of Physiology-Endocrinology and Metabolism. (2009). doi:10.1152/ajpendo.00099.2009.
- [32] S. Romeo, J. Kozlitina, C. Xing, A. Pertsemlidis, D. Cox, L.A. Pennacchio, E. Boerwinkle, J.C. Cohen, H.H. Hobbs, Genetic variation in PNPLA3 confers susceptibility to

- nonalcoholic fatty liver disease, Nature Genetics. (2008). doi:10.1038/ng.257.
- [33] S. Gerbig, Z. Takáts, Analysis of triglycerides in food items by desorption electrospray ionization mass spectrometry, Rapid Communications in Mass Spectrometry. (2010). doi:10.1002/rcm.4630.
- [34] A.U. Jackson, T. Shum, E. Sokol, A. Dill, R.G. Cooks, Enhanced detection of olefins using ambient ionization mass spectrometry: Ag+ adducts of biologically relevant alkenes, Analytical and Bioanalytical Chemistry. (2011). doi:10.1007/s00216-010-4349-5.
- [35] C. Wang, F. Yue, S. Kuang, Muscle Histology Characterization Using H&E Staining and Muscle Fiber Type Classification Using Immunofluorescence Staining, BIO-PROTOCOL. (2017). doi:10.21769/bioprotoc.2279.
- [36] S.N. Nguyen, R.L. Sontag, J.P. Carson, R.A. Corley, C. Ansong, J. Laskin, Towards High-Resolution Tissue Imaging Using Nanospray Desorption Electrospray Ionization Mass Spectrometry Coupled to Shear Force Microscopy, Journal of the American Society for Mass Spectrometry. (2018). doi:10.1007/s13361-017-1750-8.
- [37] R. Yin, J. Kyle, K. Burnum-Johnson, K.J. Bloodsworth, L. Sussel, C. Ansong, J. Laskin, High Spatial Resolution Imaging of Mouse Pancreatic Islets Using Nanospray Desorption Electrospray Ionization Mass Spectrometry, Analytical Chemistry. (2018). doi:10.1021/acs.analchem.8b00161.
- [38] E. Cequier-Sánchez, C. Rodríguez, Á.G. Ravelo, R. Zárate, Dichloromethane as a solvent for lipid extraction and assessment of lipid classes and fatty acids from samples of different natures, Journal of Agricultural and Food Chemistry. (2008). doi:10.1021/jf073471e.
- [39] J. Watrous, P. Roach, B. Heath, T. Alexandrov, J. Laskin, P.C. Dorrestein, Metabolic profiling directly from the petri dish using nanospray desorption electrospray ionization imaging mass spectrometry, Analytical Chemistry. (2013). doi:10.1021/ac4023154.
- [40] P.A. Eckert, P.J. Roach, A. Laskin, J. Laskin, Chemical characterization of crude petroleum using nanospray desorption electrospray ionization coupled with high-resolution mass spectrometry, Analytical Chemistry. (2012). doi:10.1021/ac202801g.
- [41] N.B. Cech, C.G. Enke, Practical implications of some recent studies in electrospray ionization fundamentals, Mass Spectrometry Reviews. (2001). doi:10.1002/mas.10008.
- [42] R.A. Gaiser, A. Pessia, Z. Ateeb, H. Davanian, C. Fernández Moro, H. Alkharaan, K. Healy, S. Ghazi, U. Arnelo, R. Valente, V. Velagapudi, M. Sällberg Chen, M. Del Chiaro, Integrated targeted metabolomic and lipidomic analysis: A novel approach to classifying early cystic precursors to invasive pancreatic cancer, Scientific Reports. 9 (2019) 10208. doi:10.1038/s41598-019-46634-6.
- [43] K. Contrepois, S. Mahmoudi, B.K. Ubhi, K. Papsdorf, D. Hornburg, A. Brunet, M. Snyder, Cross-Platform Comparison of Untargeted and Targeted Lipidomics Approaches on Aging Mouse Plasma, Scientific Reports. (2018). doi:10.1038/s41598-018-35807-4.
- [44] C. Wu, D.R. Ifa, N.E. Manicke, R.G. Cooks, Rapid, direct analysis of cholesterol by charge labeling in reactive desorption electrospray ionization, Analytical Chemistry. (2009). doi:10.1021/ac901003u.
- [45] M. Girod, E. Moyano, D.I. Campbell, R.G. Cooks, Accelerated bimolecular reactions in microdroplets studied by desorption electrospray ionization mass spectrometry, Chemical

- Science. (2011). doi:10.1039/c0sc00416b.
- [46] J. Laskin, P.A. Eckert, P.J. Roach, B.S. Heath, S.A. Nizkorodov, A. Laskin, Chemical analysis of complex organic mixtures using reactive nanospray desorption electrospray ionization mass spectrometry, Analytical Chemistry. (2012). doi:10.1021/ac301533z.
- [47] N. Goto-Inoue, M. Morisasa, K. Machida, Y. Furuichi, N.L. Fujii, S. Miura, T. Mori, Characterization of myofiber-type-specific molecules using mass spectrometry imaging, Rapid Communications in Mass Spectrometry. (2019). doi:10.1002/rcm.8319.
- [48] Y.H. Tsai, T.J. Garrett, C.S. Carter, R.A. Yost, Metabolomic analysis of oxidative and glycolytic skeletal muscles by matrix-assisted laser desorption/ionizationmass spectrometric imaging (MALDI MSI), Journal of the American Society for Mass Spectrometry. (2015). doi:10.1007/s13361-015-1133-y.
- [49] I. Lanekoff, K. Burnum-Johnson, M. Thomas, J. Short, J.P. Carson, J. Cha, S.K. Dey, P. Yang, M.C. Prieto Conaway, J. Laskin, High-speed tandem mass spectrometric in situ imaging by nanospray desorption electrospray ionization mass spectrometry, Analytical Chemistry. (2013). doi:10.1021/ac401760s.
- [50] K.L. Duffin, J.D. Henion, J.J. Shieh, Electrospray and Tandem Mass Spectrometry Characterization of Acylglycerol Mixtures That Are Dissolved in Nonpolar Solvents, Analytical Chemistry. (1991). doi:10.1021/ac00017a023.

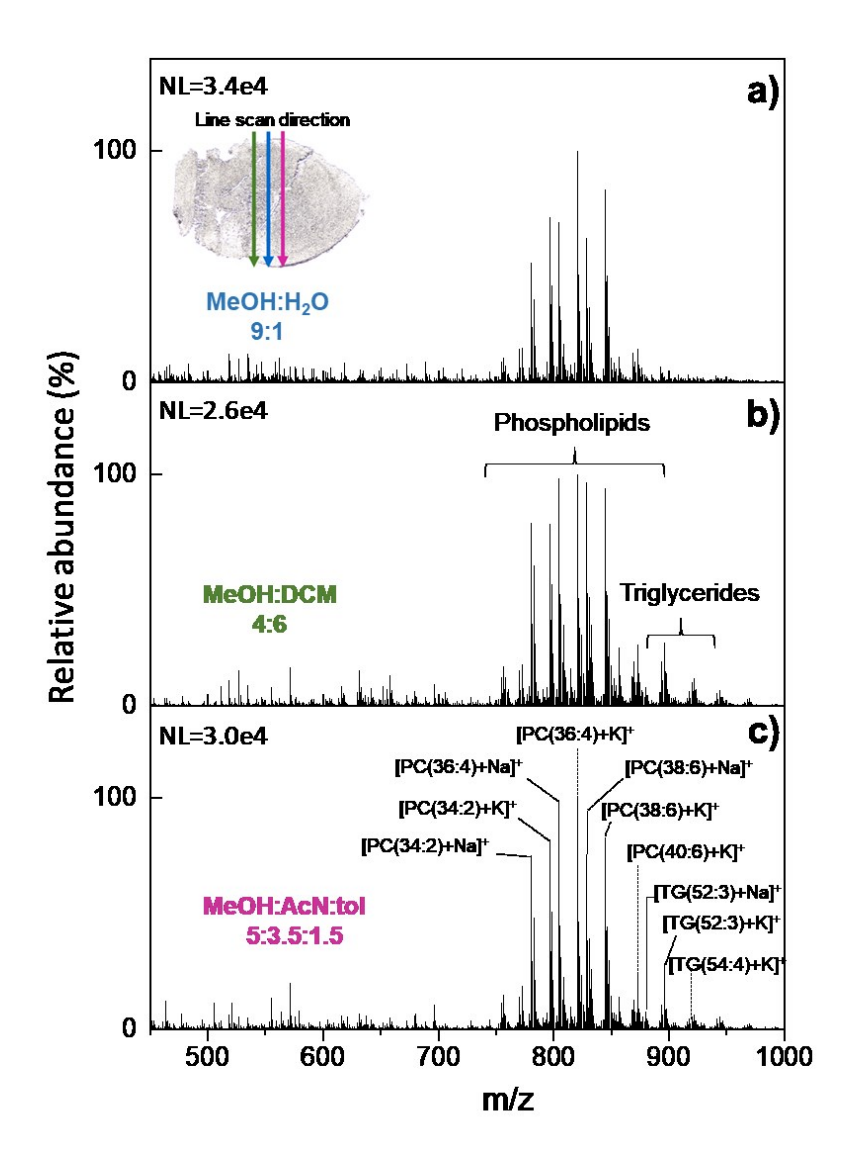


**Figure 1.** Lipid profiles obtained from a region of the line scan where TGs are abundant using a) MeOH:H<sub>2</sub>O (9:1), b) MeOH:DCM (4:6), and c) MeOH:AcN:tol (5:3.5:1.5) under the same experimental conditions. An optical image showing the region where the line scans were acquired on the tissue is displayed on the left side of panel a). Normalization factors (NL) are displayed in each panel.

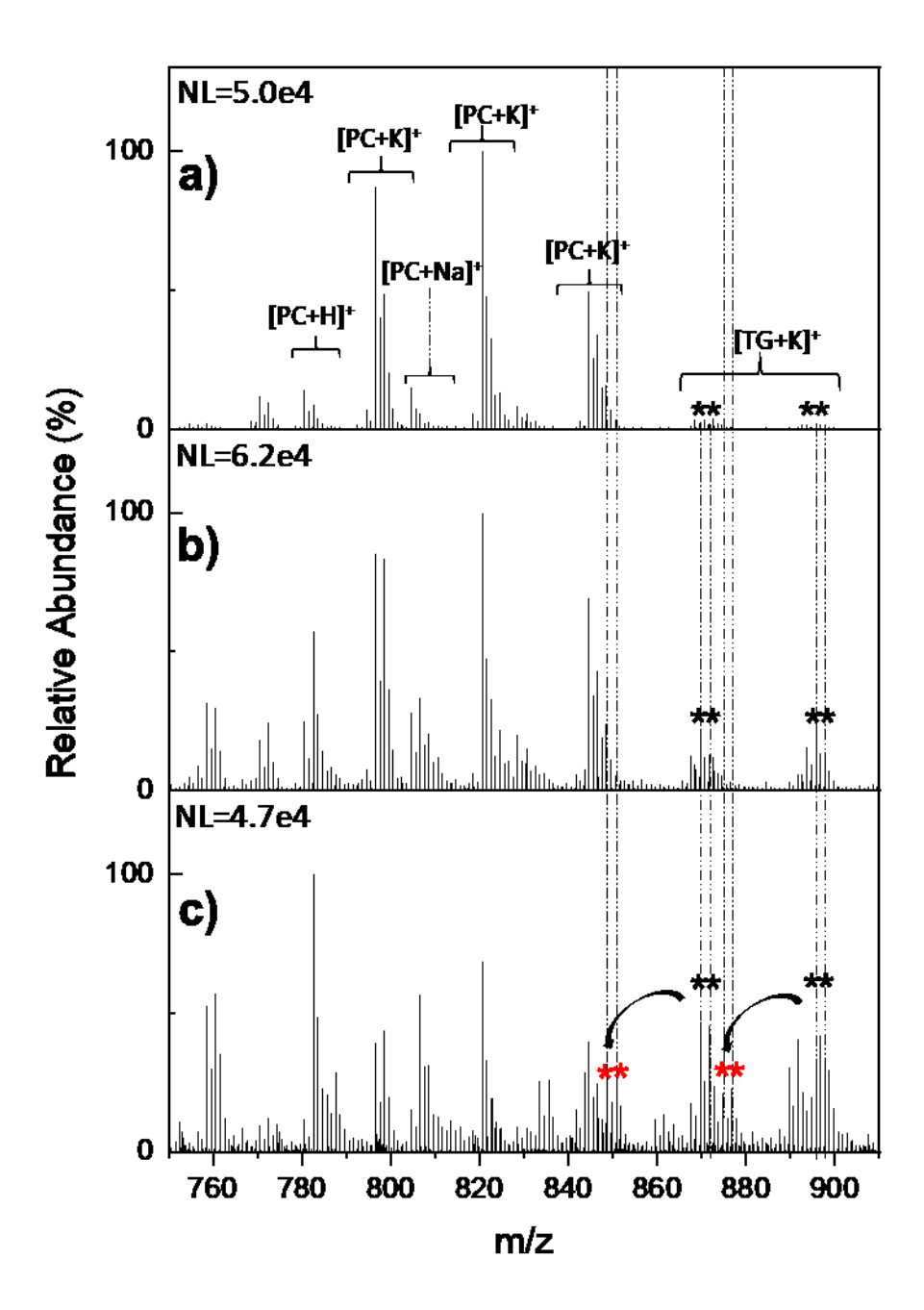


**Figure 2**. Average mass spectra of the TG-rich region displaying lipid signals obtained a) using MeOH:AcN:tol (5:3.5:1.5) and by doping MeOH:AcN:tol (5:3.5:1.5) with b) 0.1 mM and c) 2 mM of ammonium formate. Black and red asterisks highlight the same TG species detected as [M+K]<sup>+</sup> and [M+NH<sub>4</sub>]<sup>+</sup> adducts, respectively. NL values are displayed in each panel.

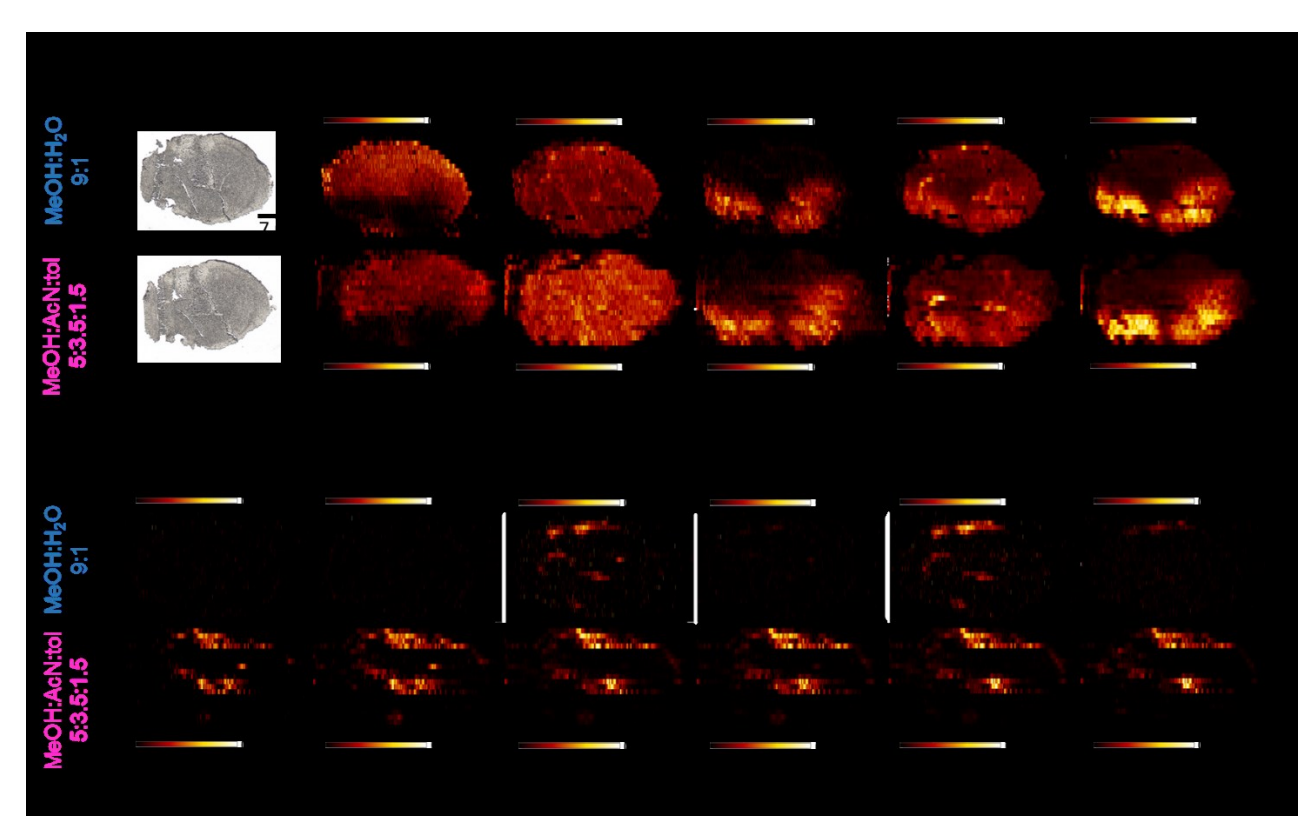


**Figure 3.** Nano-DESI images acquired using MeOH:H<sub>2</sub>O (9:1) and MeOH:AcN:tol (5:3.5:1.5) solvents in positive mode. a) Optical images of gastrocnemius tissue sections and ion images of [M+H]<sup>+</sup> ion of CAR(14:0) and carnosine, LPC (16:0), PC (36:1) and PC(40:6) detected as [M+K]<sup>+</sup> adducts. b) Ion images of TG(46:0), TG(48:0), TG(50:2), TG(50:1), TG(52:3) and TG(54:4) detected as [M+K]<sup>+</sup> adducts. Scale bar is 7 mm. All ion images are normalized to the TIC and the corresponding normalized ion abundance scales are shown in the color bars located next to each ion image.

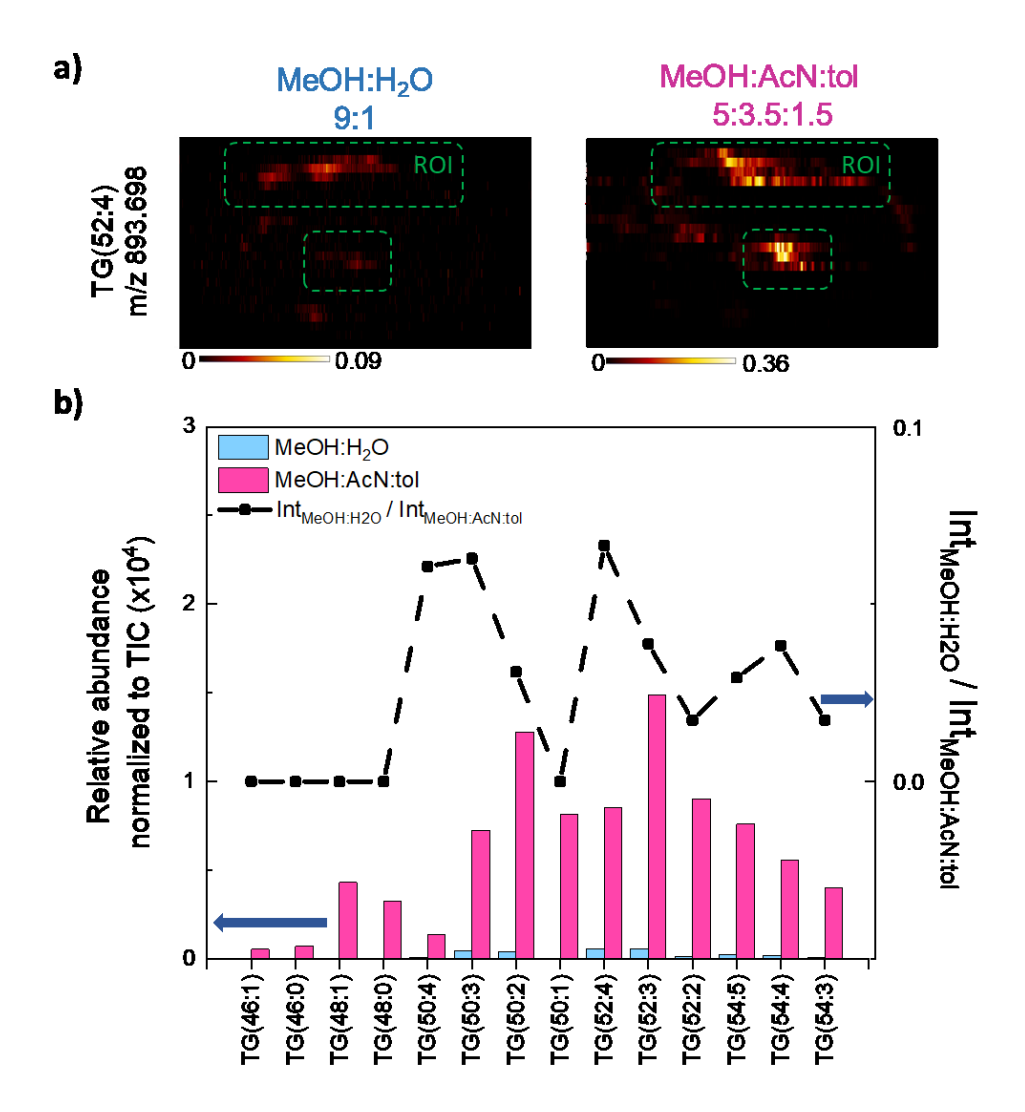


**Figure 4**. a) Ion images of TG(52:4) obtained using MeOH:H<sub>2</sub>O (9:1) and MeOH:ACN:tol (5:3.5:1.5) solvents illustrating the region of interest (ROI) analysis. Dashed green lines outline the ROI selected in each image. Color bars show the normalized ion abundance scale for each ion image. b) Bar graphs show normalized ion abundances of TGs detected as [M+K]<sup>+</sup> adducts (left axis) calculated from the average ROI spectra obtained for both images. A scatter plot shows the ratio of the abundances (right axis), Int<sub>MeOH:H2O</sub>/ Int<sub>MeOH:AcN:tol</sub>, observed for different TG species.